Multifilament structures in relativistic self-focusing

F. Cattani,[1] A. Kim,[2] D. Anderson,[1] and M. Lisak[1]
[1]*Department of Electromagnetics, Chalmers University of Technology, 412 96 Göteborg, Sweden*
[2]*Institute of Applied Physics, Russian Academy of Sciences, 603600 Nizhny Novgorod, Russia*
(Received 19 December 2000; published 26 June 2001)

A simple model is derived to prove the multifilament structure of relativistic self-focusing with ultraintense lasers. Exact analytical solutions describing the transverse structure of waveguide channels with electron cavitation, for which both the relativistic and ponderomotive nonlinearities are taken into account, are presented.

DOI: 10.1103/PhysRevE.64.016412 PACS number(s): 52.38.−r, 52.35.Mw, 42.65.Jx, 52.27.Ny

I. INTRODUCTION

Recent development in laser technology has opened up the possibility of exploring previously unattainable regimes of laser-plasma interaction [1]. Intensities of the order of 10^{18} W/cm^2 and higher can now be achieved, implying that goals like compact sources for x-ray laser [2], the fast ignitor concept for inertial confinement fusion (ICF) [3], and laser-plasma based accelerators [4] might soon be within reach. However, a major effort is still required both numerically and analytically in order to understand the nonlinear phenomena that arise in the presence of such extremely high intensities of electromagnetic radiation. Good analytical insight is also needed in order to make numerical simulations possible and to interpret their results [5].

One of the problems that have received particular attention is the combined effect of relativistic and striction (ponderomotive) nonlinearities, which occur in the propagation of superintense laser pulses through underdense plasmas [i.e., plasmas with $\omega_p < \omega$, where $\omega_p = (4\pi n_e e^2/m_e)^{1/2}$ is the plasma frequency and ω is the laser carrier frequency] [6]. This problem is not fully understood yet and there is need of a self-consistent analytical description that does not violate global charge conservation and plasma quasineutrality when describing self-focusing and self-channeling [7].

A common feature in the above mentioned schemes is that transport of laser radiation over considerable distances, well beyond the diffraction limit, and without significant energy losses is required. In achieving this goal, nonlinear self-focusing and self-channeling play an important role. Under the action of an intense laser pulse, electrons tend to be redistributed in the transverse direction as an effect of the ponderomotive pressure, the self-channeling phenomenon. The subsequent self-modification of the radial profile of the refractive index is at the origin of the nonlinear self-focusing and filamentation of the laser pulse. Nonlinear self-focusing and self-channeling offer a possibility for optical guiding of laser pulses in underdense pulses such as, for instance, the underdense corona of an ICF target, through the formation of ''hollow channels'' [8], as experimentally observed by several groups [9,10].

As was shown in [11], relativistic self-focusing shows qualitatively different features for ultraintense lasers. The ponderomotive force of superstrong fields expels electrons, thus producing ''vacuum channels'' that guide the radiation, and stable channeling with power higher than the critical one can take place [12]. However, as noticed in [11,13], analytical descriptions led to the appearance of negative electron densities. This problem was solved by setting the channel boundary positions exactly at the point where the electron density became zero. Feit *et al.* [7] showed that this procedure did not conserve the global charge and proposed including the electron temperature effect, which, however, was not self-consistently evaluated (the temperature was assumed to be derived from experimental conditions). Recently, we noted that for an overdense plasma a self-consistent description of self-induced transparency is possible that automatically takes into account global charge conservation through Poisson's equation [14]. The strong analogies between one-dimensional (1D) overdense and 2D underdense plasmas allow for an exact analysis of the stationary stage of electron cavitation due to the joint effects of relativistic and striction nonlinearities in underdense plasmas. This analysis leads to an exact analytical description of the transverse structures generated by relativistic self-focusing and also demonstrates its multifilament nature.

Depending on the incident power and intensity distribution, several qualitatively different solutions may occur. Our aim is to give an exact analytical description of the stationary stage of the fundamental configurations. We will show that, if the incident power is relatively low and the intensity has its maximum on axis, the plasma will react by generating a stationary stage with a single channel acting as an optical guide for the propagating radiation. If the incident power is increased and the intensity instead has its minimum on axis (a higher order laser mode), then the final stationary stage will display two symmetric channels. Finally, for even higher incident powers and maximum on-axis incident intensities, three channels will be generated, and so on, with the critical power for channel formation depending on the unperturbed plasma density and the wave number of the propagating radiation. Of particular interest is the fact that these structures can be interpreted as the final stationary stage of the filamentation instability, as shown by the numerical simulations presented in [5].

In this paper, we introduce in Sec. II the model equations and the approximations we will use to describe electron cavitation in a two-dimensional underdense plasma. The general is discussed in Sec. III and our results for single- and multichannel structures in 2D planar geometry are presented in the following sections, following a brief discussion of the physical mechanisms behind the generation of such structures. Finally, some conclusions are summarized in Sec. VI.

 ©2001 The American Physical Society

II. THE MODEL

Let us consider the propagation of electromagnetic radiation in a homogeneous plasma. A complete description is based on Maxwell's equations for the propagating laser radiation plus a model describing the plasma response. For the problem of interest, an important simplification comes from the physical context. Considering short pulses with length τ such that $\omega_{pe}^{-1} \ll \tau \ll \omega_{pi}^{-1}$, the ion dynamics can be neglected [12]. Furthermore, we will not be concerned with wake field generation [13], since the pulse is long enough to allow us to disregard longitudinal charge separation [7]. Finally, all thermal effects will be disregarded since, at these high intensities, electrons are driven to relativistic velocities in just a few optical cycles and the electron pressure gradient is negligible compared to the ponderomotive pressure [15].

These assumptions define the model we are using to describe our plasma. The ions are considered as an immobile neutralizing background and the electrons as a cold relativistic fluid. Our set of self-consistent equations derived from Maxwell's equations and the equation of motion for the electron component, assuming the Coulomb gauge, reads

$$\nabla^2 \mathbf{A} - \frac{1}{c^2}\frac{\partial^2 \mathbf{A}}{\partial t^2} = \frac{1}{c}\frac{\partial}{\partial t}\nabla\varphi + \frac{4\pi}{c} N e \mathbf{v}, \tag{1}$$

$$\nabla^2 \varphi = 4\pi e (N - N_0), \tag{2}$$

$$m\gamma \mathbf{v} = \frac{e}{c}\mathbf{A} + \nabla\psi, \tag{3}$$

$$\frac{\partial \psi}{\partial t} = e\varphi - mc^2(\gamma - 1), \tag{4}$$

$$\nabla \cdot \mathbf{A} = 0. \tag{5}$$

Here $\gamma = 1/\sqrt{1 - \mathbf{v}^2/c^2}$ is the relativistic factor, N is the electron density, N_0 is the equilibrium density, $-e$ and m are the electron charge and mass, respectively, $\mathbf{A}$ is the electromagnetic vector potential, φ is the electrostatic scalar potential and ψ is a scalar function that expresses the electron canonical momentum. Details of the derivation of this model can be found in [8]. Equations (3) and (4) imply that we are assuming vortex-free motion of the electrons. Taking the divergence of Eq. (1) and using Eqs. (2) and (5) we find that the charge conservation law

$$\frac{\partial N}{\partial t} + \nabla \cdot (N\mathbf{v}) = 0 \tag{6}$$

is automatically satisfied, i.e., the total charge is conserved. However, when dealing with necessarily simplified models describing the stationary regime in the presence of electron cavitation phenomena, the condition of plasma quasineutrality is not obviously conserved [11–13]. This point must be carefully discussed when constructing solutions and it will lead to the breaking of the Hamiltonian model, thus allowing for multifilament structures.

The assumption made on the pulse duration implies that the electron fluid has time to approach a quasi-steady-state [16]. Therefore, it is interesting to describe what kind of stationary state the system will reach, neglecting any transient phenomena. This leads to further simplification, because we can neglect the time dependence in Eq. (4) and, since $\mathbf{v}$ before the passage of the laser pulse must be zero, it follows from Eqs. (3) and (4) that $\psi = 0$.

In order to single out the fast optical time scale we adopt the slowly varying envelope approximation, factorizing the normalized vector potential as

$$\frac{e\mathbf{A}}{mc^2} = a_\perp(\mathbf{r}_\perp)\mathbf{r}_\perp \exp[i(hz - \omega t)] + \text{c.c.} \tag{7}$$

Assuming the paraxial approximation $k_\perp \ll h$, where $k_\perp$ is the transverse component of the laser wave number and h is the propagation constant, the parallel component of the vector potential is negligible if compared to the transverse ones and the incident radiation may be assumed to be circularly polarized without loss of generality. In what follows, we will drop the subscript denoting the perpendicular component of the various quantities. The resulting system of equations, after a few algebraic manipulations, is

$$\nabla^2 a + \left(1 - \frac{\alpha n}{\gamma}\right) a = 0, \tag{8}$$

$$\nabla^2 \phi = \alpha(n - 1), \tag{9}$$

$$\phi = \gamma - 1 \quad \text{if and only if} \quad n \neq 0, \tag{10}$$

$$\gamma = \sqrt{1 + a^2}, \tag{11}$$

where

$$\alpha = \frac{n_0}{1 - h^2/k^2}, \tag{12}$$

$k = \omega/c$ is the vacuum wave number and we have introduced the normalization $n_0 = N_0/N_{cr}$ with $N_{cr} = m\omega^2/(4\pi e^2)$, $n = N/N_0$, $\phi = e\varphi/(mc^2)$, $\mathbf{r} = k\sqrt{1 - h^2/k^2}\,\mathbf{r}_\perp$.

III. GENERAL ANALYSIS

Let us consider a two-dimensional geometry for a plasma extending in the z direction, i.e., along the laser propagation direction. We will restrict ourselves to a 1D transverse model in order to emphasize the main features of multifilament structures. In Eqs. (8)–(11) the propagation constant h plays the role of a free parameter which, together with the background plasma density n_0, defines what kind of filament structures can be realized as a final state of the self-focusing evolution. In reality, it would depend on several parameters and factors such as the laser power, the geometrical configuration (the angle of focusing, for instance), and the prehistory of the process.

The self-channeling we are interested in is realized only when $\alpha > 1$, i.e., for underdense plasmas when $1 > h/k$

$>\sqrt{1-n_0}$ and for overdense plasmas with $n_0>1$ when $h/k<1$.

The complete mathematical analogy between the present model and the one introduced in [17] suggests that our plasma will react to the laser action with the formation of regions depleted of electrons, where the laser electromagnetic radiation is trapped, a consequence of the well known phenomenon of electron cavitation and channeling. Electrons tend to be expelled from the focal spot by the laser ponderomotive force and, at the same time, under such extreme conditions, they acquire relativistic quiver velocities. These effects both contribute to a self-induced modification of the radial profile of the refractive index and a consequent nonlinear trapping of the laser radiation in finite plasma regions. This modification is the basic mechanism in the optical guiding of laser pulses in plasmas. It is possible to give an exact analytical description of the asymptotic stationary plasma-field structures generated in the transverse direction for different values of α. As we will see, these structures consist of one or more channels, depending on the corresponding incident power. The most delicate point in the analysis will be the determination of such structures complying with global charge conservation.

Equations (8)–(11) were analyzed in detail in [13] and also in [18] with respect to both underdense and overdense plasmas and solutions were found in the form of continuous functions. Fundamental to those analysis is the Hamiltonian structure of the set of equations (8)–(11), which reads

$$\mathcal{H}_E=\frac{1}{2(1+a^2)}a'^2-\frac{1}{2}(2\alpha\sqrt{1+a^2}-a^2), \tag{13}$$

where the prime denotes the derivative with respect to the transverse coordinate x. As $n(x)\to 1$ and both $a(x)$ and $a'(x)$ vanish for $x\to\infty$, the integral of motion equals

$$\mathcal{H}_E=\mathcal{H}_{E0}\equiv-\alpha. \tag{14}$$

It follows that there is an exact solitonlike analytical solution given by

$$a(x)=\frac{A_m\cosh[|\varepsilon_0|^{1/2}(x-x^{(0)})]}{\alpha\cosh^2[|\varepsilon_0|^{1/2}(x-x^{(0)})]-|\varepsilon_0|} \tag{15}$$

where $\varepsilon_0=1-\alpha$ and the parameter $x^{(0)}$ defines the peak position of the function (15), which is given by $A_m=2[\alpha(\alpha-1)]^{1/2}$. Once this solution is known, we also have a description for the electron density through Poisson's equation (9) and the equation of motion (10):

$$n=3(1+a^2)+2\frac{\sqrt{1+a^2}}{\alpha}(\mathcal{H}_E-a^2). \tag{16}$$

The minimum electron density in a cavity is given by $n_{min}=1-4(\alpha-1)^2$, which implies that, for $\alpha>1.5$, this solution leads to the unphysical result of a negative electron density. Therefore, if $\alpha\leqslant 1.5$, i.e., for propagation constants lying in the interval $\sqrt{1-2n_0/3}\geqslant h/k>\sqrt{1-n_0}$, we have solutions expressed by the continuous functions (15) and (16).

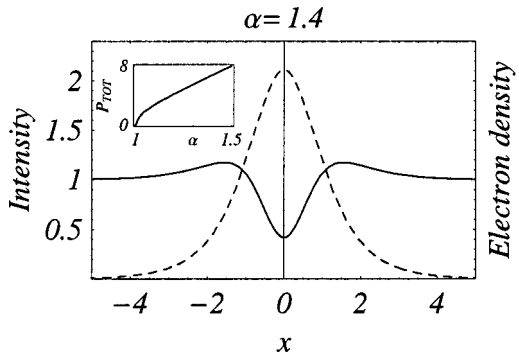

FIG. 1. Plasma-field structures (dashed line) and electron density distribution (continuous line) for the case of a single filament in an underdense plasma, for a fixed value of α less then 1.5. In this case $\alpha=1.4$. The power needed to generate a single-filament structure is shown in the inset as a function of the parameter α for α less then 1.5. All quantities are dimensionless.

The field and density structures and the corresponding power related to the propagation constant are presented in Fig. 1. It should be emphasized that, for $\alpha\leqslant 1.5$, since the system is fully described by the Hamiltonian (13), there are no other structures except this single-filament one. The important question is what will happen for higher incident powers or, in other words, for $\alpha>1.5$. The procedure for constructing a solution followed in [11,12,15], which consisted in assuming the electron density to vanish within the interval where the solution for the density (16) is negative, led to nonconservation of the global charge. However, what is happening is that the ponderomotive force is pushing electrons away from the central axis, while the force due to charge separation acts in the opposite direction. Thus, when an equilibrium is reached, we have the formation of a stationary structure consisting of a channel emptied of its electrons. This means that the global structure of the solution consists of two parts, the first one described by the Hamiltonian (13), while the second, describing the depletion regions where the electron density vanishes, has the typical vacuum Hamiltonian:

$$\mathcal{H}_V=\frac{1}{2}(a'^2+a^2). \tag{17}$$

In Fig. 2 the phase portrait of the full system is presented for the single-filament case with $\alpha=2$ while in Fig. 3 the same phase portrait is shown for a more complicated multifilament case with $\alpha=2$.

The continuous solitonlike solution described by Eq. (15) corresponds here to the separatrix trajectory and its starting and final point is $a=0$, $a'=0$. As pointed out, this solution breaks down for higher values of α and we indicate on the phase portrait the curve beyond which the electron density (16) formally becomes negative.

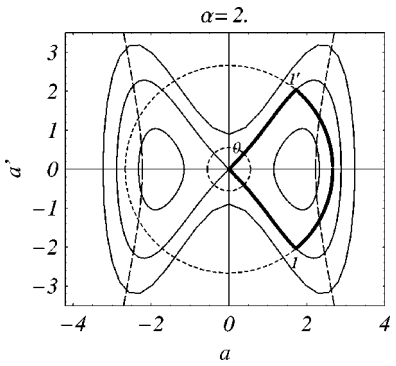

FIG. 2. Phase portrait for a system that develops a single-filament structure. The thick line represents the trajectory followed by the system, starting from the separatrix at $a=0$, $a'=0$, then moving on along the vacuum trajectory to finally come back to the starting point along the separatrix again, which represents the symmetrical plasma region. The corresponding plasma-field structures are illustrated in Fig. 4 below.

Beyond the limit curve for the electron density we have to introduce the ''vacuum'' part of the solution. Our system has left the separatrix and has started to move along the vacuum trajectory. The boundary position up to which the electrons are displaced is determined by the equilibrium condition between the two forces acting on them, as described by the equation of motion

$$\phi' = \gamma' \tag{18}$$

and by the conservation of the total charge, which means that, in order to conserve the total charge, the boundary positions can now be determined by inserting the equilibrium condition (18) into Poisson's equation and integrating it.

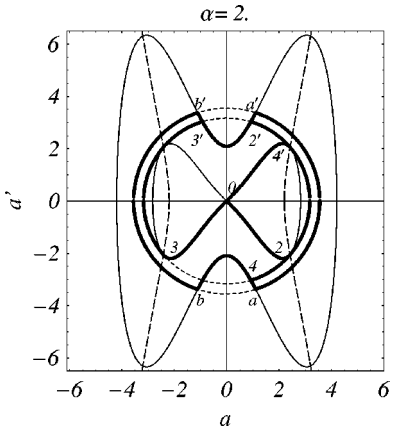

FIG. 3. Phase portrait for a more complicated case with multiple filaments. The thick line represents the trajectory in the case of four filaments. Solid lines represent trajectories relative to electron layers while dashed lines are relative to depletion regions and the long dashed lines separate regions with positive and negative electron density, as follows from Eq. (16).

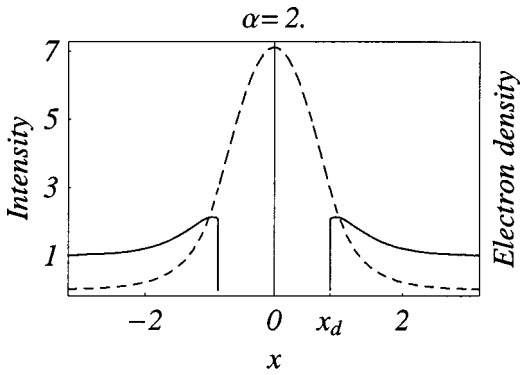

FIG. 4. Plasma-field structures (dashed line) and electron density distribution (continuous line) for the case of a single channel for a fixed value of $\alpha=2$. All quantities are dimensionless.

IV. SINGLE-FILAMENT SOLUTIONS

Let us consider a localized solution with one peak for the intensity. Its structure is defined by the closed trajectory (0-1-1′-0) shown in Fig. 2. We will treat this kind of solution as a single-filament solution.

Integrating Poisson's equation over the whole interval we obtain

$$x_d = -\frac{1}{\alpha}\frac{a_d a_d'}{\sqrt{1+a_d^2}}, \tag{19}$$

where a_d is the field amplitude at the boundary position x_d. At the same time, we have to match the field in the vacuum channel

$$a(x) = A_V \cos x \tag{20}$$

and its first derivative to the field and its first derivative in the plasma region, that is,

$$A_V^2 = a_d^2 + a_d'^2 \tag{21}$$

and

$$x_d = -\arctan\left(\frac{a_d'}{a_d}\right). \tag{22}$$

Given the integral of motion $\mathcal{H}_E = -\alpha$, from the two equations for x_d we obtain a transcendental equation for the boundary amplitude a_d,

$$\tan\left(\frac{a_d[2\alpha(\sqrt{1+a_d^2}-1)-a_d^2]^{1/2}}{\alpha}\right) = \frac{\sqrt{1+a_d^2}}{a_d}[2\alpha(\sqrt{1+a_d^2}-1)-a_d^2]^{1/2}, \tag{23}$$

which can be solved numerically, so that now we know everything about the structures generated in this case (see Fig. 4). It is important to be careful when solving this equation

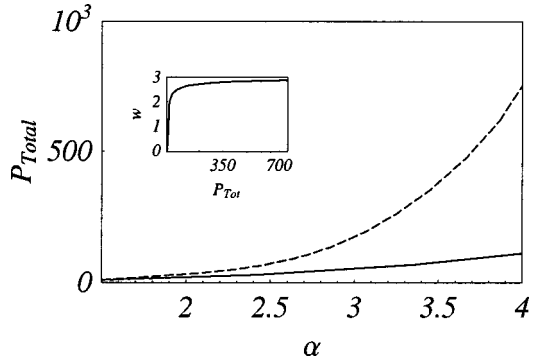

FIG. 5. Total power (continuous line) and channel width $w = 2x_d$ (inset) for the single-filament case. For comparison, the dashed line shows the total power calculated according to the commonly used model, without taking into account global charge conservation. All quantities are dimensionless.

since it has multiple solutions, but we have to choose the first that satisfies the condition of charge conservation.

The calculation of the total power for this single-channel configuration as a function of α is straightforward, $P = \int_{-\infty}^{+\infty} a^2(x)dx$, and the result is presented in Fig. 5. For comparison, we present here also the total power calculated within the previous model, when the boundary position x_d was assumed to be the one where the electron density vanished. In this case, the total charge not being conserved, there was an excess of positive charge, which led to a much higher power required in order to overcome the restoring force due to this charge excess. Consequently, the power needed to generate such structures was overestimated. It is also interesting to see how, for increasing values of α and consequently increasing values of the required power, the width of the central vacuum channel becomes larger, but, after the initial rapid growth, its increase becomes slower (see the inset in Fig. 5).

It is interesting to note that analogous structures can be found in a cylindrical geometry, although with the help of numerical computations. As this work is focused on clarifying the role of plasma neutrality when constructing structures generated by the interplay of ponderomotive and relativistic nonlinearity, the extension of these same structures to a more realistic and important axisymmetrical configuration, requiring more attention to the complications due to higher dimensionality, will be presented separately.

V. MULTIFILAMENT STRUCTURES

It is evident from our analysis that, due to the requirements of global charge conservation and to the symmetry imposed with respect to the z axis, for a fixed α the single-filament configuration and the power necessary to generate this structure are uniquely determined. If this power is exceeded, the incident electromagnetic radiation is strong enough to spread along the transverse direction of the plasma channel over a distance larger than in the previous case, but still finite. For a sufficiently strong power, the final stationary

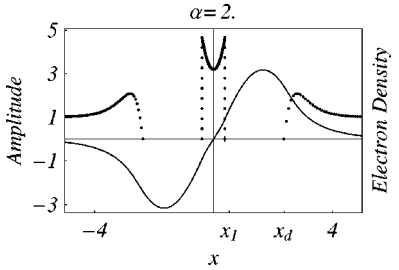

FIG. 6. Double-channel structure for a plasma with a fixed $\alpha = 2$ and maximum possible intensity a_d^2 at the last boundary (continuous line) and electron density distribution (dotted line). All quantities are dimensionless.

state will present a multiple channel structure which can again be analytically described. It is important to note that some of these structures cannot be considered as purely higher order eigenstates of the initial equations and therefore their existence and nature is not obvious. The power necessary for generating each of these structures can be exactly calculated as well. As we will show, this allows for the definition of a threshold power for the generation of multifilament structures.

Let us start with the case of an intensity distribution with a minimum on the symmetry axis. An example of the trajectory in the phase space for the double-channel case is given in Fig. 3, indicated as (0-2-2′-3′-3-0). To construct the field structure we can start from inside the plasma region at $x \to +\infty$, where we know the integral of motion and the expression for the decaying field and the electron density [see Eqs. (15) and (16), respectively]. When we come to the depletion region there is a certain freedom in the choice of the boundary amplitude a_d, as we are going backward from the last plasma region toward the central axis. The only requirement for a_d is that the electron density must not be negative; therefore we can fix the boundary amplitude (and therefore the boundary position x_d as well) to any value up to a maximum for which the density at the boundary vanishes. This means that for a fixed α the two-peak solution is not unique and there is a certain power range for generating such a structure. For a given a_d the field in the vacuum region,

$$a(x) = A_V \cos(x - \varphi), \tag{24}$$

is completely determined from the matching conditions, but now the vacuum channel extends from the x_d to a certain x_1 (see Fig. 6) which is to be determined taking into account charge conservation.

In order to construct a structure with only one degree of complexity more than for the single channel, we stop at the next plasma layer, which will be centered on the symmetry axis. An analytical expression for the field in this central plasma layer can be derived by solving the equation for the vector potential. Now the solution is not localized as before, and therefore the boundary conditions and the Hamiltonian $\mathcal{H}_E = \mathcal{H}_{E1} > -\alpha$ are not known. The solution is expressed in terms of two-parameter elliptic functions as

$$a(x)=\begin{cases}\dfrac{2q\,\mathrm{cn}[\varepsilon_1^{1/2}(x-x^{(1)})]}{2+[(q^2+1)^{1/2}-1]\mathrm{sn}^2[\varepsilon_1^{1/2}(x-x^{(1)})]}, & -\alpha<\mathcal{H}_{E1}<\alpha \\ \dfrac{2\bar{q}\,\mathrm{sn}\{[(\varepsilon_1+1)^2-\alpha^2]^{1/2}(x-x^{(1)})/2\}}{\bar{q}^2-\mathrm{sn}^2\{[(\varepsilon_1+1)^2-\alpha^2]^{1/2}(x-x^{(1)})/2\}}, & \mathcal{H}_{E1}>\alpha,\end{cases} \tag{25}$$

where $\varepsilon_1=(\alpha^2+1+2\mathcal{H}_{E1})^{1/2}$, $q=[(\varepsilon_1+\alpha)^2-1]^{1/2}$ and $\bar{q}=[(\varepsilon_1+\alpha+1)/(\varepsilon_1+\alpha-1)]^{1/2}$, while $k=\{[\alpha^2-(\varepsilon_1-1)^2]/4\varepsilon_1\}^{1/2}$ and $\bar{k}=\{[(\varepsilon_1-1)^2-\alpha^2]/(\varepsilon_1+1)^2-\alpha^2)\}^{1/2}$ are the moduli of the elliptic integrals of the first kind, respectively, for the two cases. These solutions were presented in [14] for the problem of self-induced transparency of an overdense plasma. Imposing the conservation of the total charge by integrating Poisson's equation from $x=0$ to $x=\infty$ with the equilibrium condition defined by the equation of motion [see Eq. (18)], we obtain a transcendental equation for the quantity $\xi=x_1-x_d$:

$$\xi=g(\xi)-g(0), \tag{26}$$

where

$$g(\xi)=\frac{A_V^2\sin[2(\xi+\xi_0)]}{2\alpha[1+A_V^2\cos^2(\xi+\xi_0)]^{1/2}}, \quad \xi_0=-\arctan\left(\frac{a_d'}{a_d}\right). \tag{27}$$

The solution of this equation gives a complete description of the vacuum layer since x_d is already determined. A necessary condition for this equation to have a nontrivial solution is that $g'(\xi=-\xi_0)>1$, i.e.,

$$g'(\xi=-\xi_0)=\frac{A_V^2}{\alpha(1+A_V^2)^{1/2}}>1, \tag{28}$$

which cannot be satisfied unless $\alpha\geqslant 1.5$. This leads to the conclusion that if $\alpha<1.5$, that is, if the propagation constant of the wave vector h is not large enough, our system will never reach a stationary state and it will display only a dynamical behavior with the electromagnetic perturbation propagating along the transverse direction. Otherwise, we can numerically calculate how the minimum boundary intensity such that Eq. (26) still has a solution depends on α and also find a solution of this equation and calculate x_1. To finally obtain a complete description of the central plasma layer we only have to apply the boundary conditions at x_1 to determine the parameters that are still unknown, $\mathcal{H}_{E1}$ and $x^{(1)}$, while the symmetry axis is determined as the symmetry axis of the elliptic function. In Fig. 6 a double-channel structure is shown for fixed α and for maximum amplitude at the last boundary (so that the electron density at this boundary vanishes). It should be noted that, for a fixed value of the boundary amplitude a_d, the width of the vacuum channels and the peak intensity in these channels increase with α. Furthermore, the maximum possible boundary amplitude itself is an increasing function of α and, for any given value of this parameter, such a maximum amplitude determines the maximum power we can deliver to the plasma in order to generate a double-channel structure. Exceeding this maximum power will force the system to generate a structure with one more filament and therefore we can talk about a threshold power for the generation of multi-filament structures.

In Fig. 7 we show P_{Total} calculated for varying α and for a_d fixed to its maximum possible value. In the inset is shown instead how the total power varies with the intensity at the last boundary. The apparently anomalous behavior for low boundary intensities is due to the fact that the left branch corresponds to a different kind of two-filament solution whose phase portrait and field structures are presented in Figs. 8 and 9.

As can be seen following the trajectory (0-2-2′-3′-3-0), in this case the field amplitude, once it leaves the separatrix, never crosses the zero point until it reaches the separatrix again. For those periodic trajectories lying inside the separa-

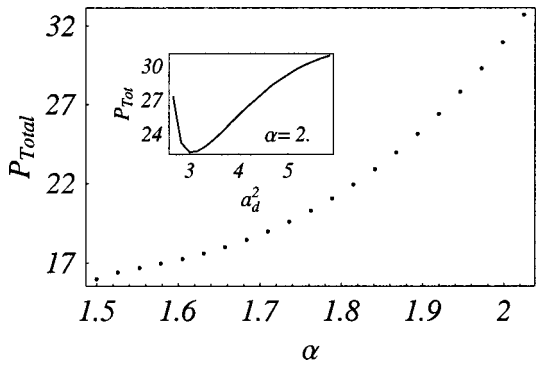

FIG. 7. Total power required to generate a double-channel structure versus α for the case of maximum possible intensity at the last boundary and (inset) as a function of the boundary intensity for fixed $\alpha=2$.

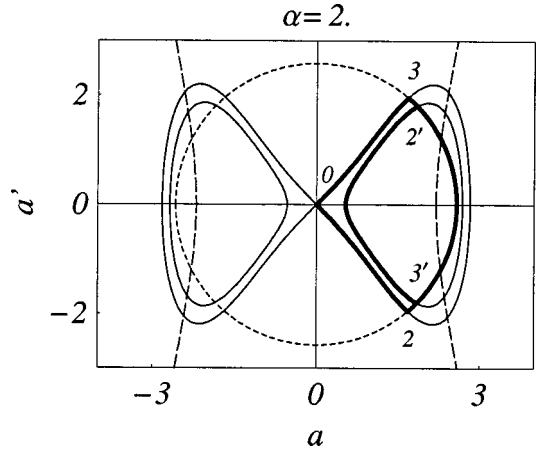

FIG. 8. Phase portrait for a system that develops a double-filament structure. In this case the field amplitude never vanishes except at $\pm\infty$ on the separatrix. The corresponding plasma-field structures are illustrated in Fig. 9.

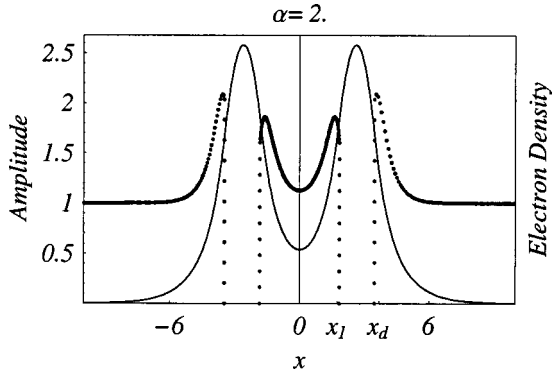

FIG. 9. Plasma-field structures for a higher order mode solution where the field amplitude never vanishes except at $\pm\infty$.

trix, the Hamiltonian $\mathcal{H}_{E1}$ is less than $-\alpha$ and the field solutions for the electron layers assume a different form and are now described in terms of elliptic functions as

$$a(x)=\frac{(\alpha-\varepsilon_1-1)\{1-(\varepsilon_1^{1/2}/\varepsilon_2)\mathrm{sn}^2[\varepsilon_2(x-x^{(1)})]\}^{1/2}}{1-2(\varepsilon_1/\alpha+\varepsilon_1-1)\mathrm{sn}^2[\varepsilon_2(x-x^{(1)})]}, \tag{29}$$

where $\varepsilon_1=(\alpha^2+1+\mathcal{H}_{E1})^{1/2}$, $\varepsilon_2=[\alpha^2-(\varepsilon_1-1)^2]/2$, and the modulus of the elliptic integral of the first kind is $k=\varepsilon_1^{1/2}/\varepsilon_2$. The procedure to define the electron cavitation boundaries is the same as the one followed previously to build the structures presented in Fig. 6.

The solution we have constructed and the corresponding choice of a closed one-cycle trajectory in the phase space is not unique. We can pass a depletion region not only at the point $3'$ to form a one cycle trajectory, but also at the point b' in order to create a periodic trajectory such as b'-b-a-a', (see Fig. 3). Following this trajectory means that we will have a new structure with new channels and plasma layers, which were not present in the double-channel structure previously described.

We would like to underline the fact that the periodic trajectory shown in Fig. 3 corresponds to a particular configuration as the points b', a', a, b are related by a complete symmetry. It is possible to see what this means by looking at the field structures described by such a trajectory (see Fig. 10): The central channels are completely symmetric; at each boundary we have the same intensity. It is again the necessity for global charge conservation that leads, by integrating Poisson's equation, to a transcendental equation for the field at the boundary of the new plasma layer:

$$\tan\left(\frac{a_d[2\mathcal{H}_{E1}+2\alpha\sqrt{1+a_d^2}-a_d^2]^{1/2}}{\alpha}\right) = \frac{\sqrt{1+a_d^2}}{a_d}[2\mathcal{H}_{E1}+2\alpha\sqrt{1+a_d^2}-a_d^2]^{1/2}. \tag{30}$$

This equation is similar to Eq. (23) but now the Hamiltonian value $\mathcal{H}_E=\mathcal{H}_{E1}$ is the one defined for the new electron layer. In the case of a single-peak field distribution, this equation had a unique solution; consequently we can add to the two-

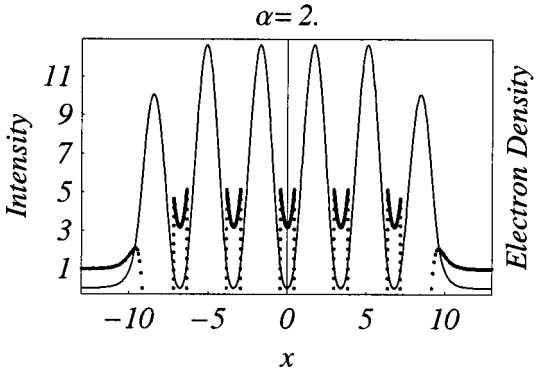

FIG. 10. Six-channel structure for a plasma with fixed $\alpha=2$ and maximum possible intensity at the last boundary (continuous line) and electron density distribution (dotted line). All quantities are dimensionless.

filament distribution whole periodic cycles, i.e., even numbers of filaments, by jumping to consecutive vacuum trajectories at the point b' or repeating the same vacuum trajectories. This is shown in Fig. 10 where a six-filament structure is presented, which corresponds to the trajectory (0-2-2′-b'-a'-a-b-3′-3-0), with two cycles along the periodic trajectory b'-a'-a-b. Again, it is important to note that this structure, completely symmetric, is peculiar to a planar geometry.

We can also add to the single-filament configuration an odd number of filaments, considering trajectories corresponding to a certain number of cycles plus half a cycle. Consider, for example, the trajectory (0-2-2′-b'-b-4-4′-0), where the points 4,4′ are symmetrical with 2′,2, respectively, which corresponds to a three-filament structure. The result is shown for a fixed value of α in Fig. 11.

Finally, in Fig. 12, we present on the same graph the calculated maximum powers as functions of α for three of the different cases we have analyzed, single, double, and triple channels. The same procedure that we have described may also be applied to the case presented in Fig. 8, where an integer number of filaments can be added since a full cycle occurs within a half space of the phase portrait. Therefore, by

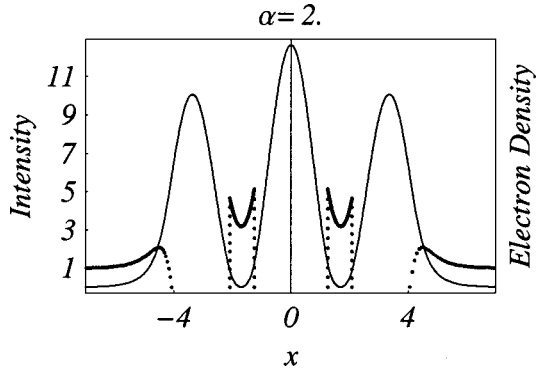

FIG. 11. Three-channel structure for a plasma with fixed $\alpha=2$ and maximum possible intensity at the last boundary (continuous line) and electron density distribution (dotted line). All quantities are dimensionless.

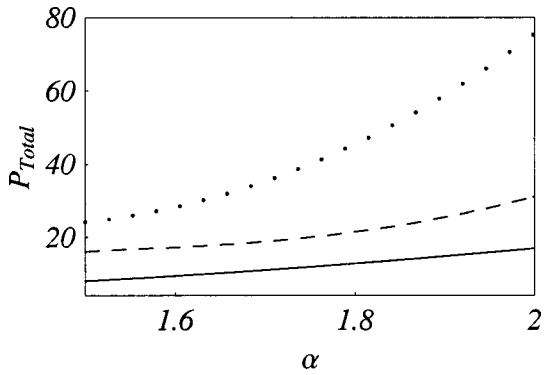

FIG. 12. Total power as a function of α for the three different cases: single channel (continuous line), double channel (dashed line), and triple channel (dotted line). In each case, the amplitude at the last boundary was chosen as the maximum possible one.

using this procedure, we can construct multifilament solutions that exist only for $\alpha > 1.5$ and represent plasma channels with electron cavitation. They differ from each other because of the laser power transported along these channels and, as there is a minimum laser power required for exciting such structures, we can define the power thresholds for creating non-single-filament structures.

VI. CONCLUDING REMARKS

In conclusion, we have presented an exact analysis of self-channeling structures generated as a consequence of relativistic self-focusing due to the interaction of ultraintense laser radiation with an underdense plasma. In this analysis, the plasma quasineutrality condition is accurately taken into consideration and this quantitatively affects some results on channeling laser power. This analysis allows us to prove the multifilament nature of the relativistic self-focusing and to calculate the threshold power for exciting multifilament structures. Such a result is not achievable in media with a local nonlinearity, like the Kerr one, because the governing equation has an overall Hamiltonian structure. In the case we have analyzed, each electron cavitation channel corresponds to a certain part of the trajectory followed by the system in the phase space, each part with its own Hamiltonian value, as shown in Fig. 2. Concerning the definition of a threshold power, it is interesting to see how filament structures with regions depleted of electrons can be generated by the interaction if the parameter α is greater than 1.5. For $\alpha \leqslant 1.5$ we have only single-filament field structures, with no depletion regions. As soon as α exceeds 1.5 there are plasma regions that are emptied of their electrons and the number of filaments thus generated increases with increasing incident power. We can therefore define the maximum power incident on a plasma with $\alpha = 1.5$ as the real threshold power for generating non-single-filament structures (see Fig. 1). The same construction procedure followed for the single-filament solution can then be easily extended to a more realistic axisymmetrical case to obtain the analogs of Figs. 4, 6, and 9, while a real 2D transverse approach is needed for the multifilament structure problem, especially for the case presented in Fig. 10, where a number of equal filaments have been added to the fundamental structure. To extend such a multifilament structure to a cylindrical geometry requires particular attention and the inclusion of an azimuthal vortex-like dependence to take into account the complication due to higher dimensionality. Therefore it is not possible to simply think of this generalization in terms of multiple ring configurations because the axial symmetry that holds for the simplest single-filament structures can be broken for more complicated cases. We would also like to note that it is reasonable to expect these structures to be fairly stable on the time scale considered, since in channels emptied of their electrons no further focusing or Raman instabilities can take place. The extreme robustness of the fundamental structures has been shown by numerical investigations; see, for example, Refs. [7], [11], and [12].

ACKNOWLEDGMENTS

This work was partly supported by INTAS (Grant No. 96-339). One of the authors (F.C.) would like to acknowledge support from the European Community (TMR program) under Contract No. ERBFMBICT972428.

[1] M. Perry and G. Mourou, Science **264**, 917 (1994).
[2] S. Y. Chen *et al.*, Phys. Rev. Lett. **84**, 5528 (2000).
[3] M. Tabak *et al.*, Phys. Plasmas **1**, 1626 (1994).
[4] E. Esarey *et al.*, IEEE Trans. Plasma Sci. **24**, 252 (1996).
[5] G. A. Askar'yan *et al.*, Pis'ma Zh. Éksp. Teor. Fiz. **60**, 240 (1994) [JETP Lett. **60**, 241 (1994)]; A. Pukhov and J. Meyer-ter-Vehn, Phys. Rev. Lett. **76**, 3975 (1996).
[6] A. G. Litvak, Zh. Éksp. Teor. Fiz. **57**, 629 (1969) [Sov. Phys. JETP **30**, 344 (1969)]; C. Max *et al.*, Phys. Rev. Lett. **33**, 209 (1974).
[7] M. D. Feit *et al.*, Phys. Rev. E **57**, 7122 (1998).
[8] X. L. Chen and R. N. Sudan, Phys. Fluids B **5**, 1336 (1993).
[9] A. B. Borisov *et al.*, Phys. Rev. Lett. **68**, 2309 (1992).
[10] P. E. Young and P. R. Bolton, Phys. Rev. Lett. **77**, 4556 (1996); M. Borghesi *et al.*, *ibid.* **78**, 879 (1997); S. Y. Chen *et al.*, *ibid.* **80**, 2610 (1998); B. La Fontaine *et al.*, Phys. Plasmas **6**, 1615 (1999); A. J. Mackinnon *et al.*, *ibid.* **6**, 2185 (1999).
[11] G. Z. Sun *et al.*, Phys. Fluids **30**, 526 (1987).
[12] A. B. Borisov *et al.*, Phys. Rev. A **45**, 5830 (1992); Plasma Phys. Controlled Fusion **37**, 569 (1995).
[13] T. Kurki-Suonio P. J. Morrison, and T. Tajima, Phys. Rev. A **40**, 3230 (1989).
[14] A. Kim *et al.*, Pis'ma Zh. Éksp. Teor. Fiz. **72**, 355 (2000) [JETP Lett. **72**, 241 (2000)].
[15] M. D. Feit *et al.*, Phys. Rev. E **53**, 1068 (1996).
[16] P. Sprangle *et al.*, Phys. Rev. Lett. **69**, 2200 (1992).
[17] F. Cattani *et al.*, Phys. Rev. E **62**, 1234 (2000).
[18] J. H. Marburger and R. F. Tooper, Phys. Rev. Lett. **35**, 1001 (1975).